

Pulmonary artery imaging under free-breathing using golden-angle radial bSSFP MRI: a proof of concept

Alexander Fyrdahl^{1,2}  | Roberto Vargas Paris^{3,4} | Sven Nyrén^{1,5} | Karen Holst^{1,2} | Martin Ugander^{1,2} | Peter Lindholm^{3,5} | Andreas Sigfridsson^{1,2}

¹ Department of Molecular Medicine and Surgery, Karolinska Institutet, Stockholm, Sweden

² Department of Clinical Physiology, Karolinska University Hospital, Stockholm, Sweden

³ Department of Physiology and Pharmacology, Karolinska Institutet, Stockholm, Sweden

⁴ Department of Radiology, Karolinska University Hospital, Stockholm, Sweden

⁵ Department of Thoracic Radiology, Karolinska University Hospital, Stockholm, Sweden

Correspondence

Andreas Sigfridsson, Department of Clinical Physiology C8:27, Karolinska Institutet and Karolinska University Hospital, Eugenivägen 23, SE-171 76 Stockholm, Sweden.
Email: andreas.sigfridsson@gmail.com

Funding information

Swedish Foundation for Strategic Research, Grant/Award number SSF ICA-120063; Stockholm County Council, Grant/Award number ALF LS 1411-1372

Purpose: To evaluate the feasibility of an improved motion and flow robust methodology for imaging the pulmonary vasculature using non-contrast-enhanced, free-breathing, golden-angle radial MRI.

Methods: Healthy volunteers ($n = 10$, age 46 ± 11 years, 50% female) and patients ($n = 2$, ages 27 and 84, both female) were imaged at 1.5 T using a Cartesian and golden-angle radial 2D balanced SSFP pulse sequence. The acquisitions were made under free breathing without contrast agent enhancement. The radial acquisitions were reconstructed at 3 temporal footprints. All series were scored from 1 to 5 for perceived diagnostic quality, artifact level, and vessel sharpness in multiple anatomical locations. In addition, vessel sharpness and blood-to-blood clot contrast were measured.

Results: Quantitative measurements showed higher vessel sharpness for golden-angle radial ($n = 76$, 0.79 ± 0.11 versus 0.71 ± 0.16 , $p < .05$). Blood-to-blood clot contrast was found to be 23% higher in golden-angle radial in the 2 patients. At comparable temporal footprints, golden-angle radial was scored higher for diagnostic quality ($\text{mean} \pm \text{SD}$, 2.3 ± 0.7 versus 2.2 ± 0.6 , $p < .01$) and vessel sharpness (2.2 ± 0.8 versus 2.1 ± 0.5 , $p < .01$), whereas the artifact level did not differ (3.0 ± 0.9 versus 3.0 ± 1.0 , $p = .80$). The ability to retrospectively choose a temporal resolution and perform sliding-window reconstructions was demonstrated in patients.

Conclusion: In pulmonary artery imaging, the motion and flow robustness of a radial trajectory does both improve image quality over Cartesian trajectory in healthy volunteers, and allows for flexible selection of temporal footprints and the ability to perform real-time sliding window reconstructions, which could potentially provide further diagnostic insight.

KEY WORDS

bSSFP, free breathing, golden angle, non-Cartesian, radial

1 | INTRODUCTION

Imaging pulmonary arteries with non-contrast-enhanced MRI has several benefits over contrast-enhanced computed tomography angiography (CTA), which is widely considered to be the modality of choice for evaluating pulmonary embolism.¹ Benefits include reducing the risks associated with exposure to ionizing radiation and the risks associated with iodinated contrast agents. The multicenter Prospective Investigation of Pulmonary Embolism Diagnosis (PIOPED) studies suggest as many as 24% of patients with suspected pulmonary embolism have some contraindication for CTA (e.g., renal dysfunction), which was observed in 19% of the cases.^{2,3} The PIOPED III study found that gadolinium-enhanced MRA (Gd-MRA) is viable for diagnosis when CTA is contraindicated.³ However, because of the characteristically bright blood signal of balanced SSFP (bSSFP), the pulmonary vessels can be imaged without the use of contrast agent enhancement. The omission of contrast agent injections eliminates the risk of poor bolus timing, potentially increasing the success rate of the study. Furthermore, many methodologies for MRI rely on breath-holding, but because dyspnea is common in the targeted patient population, a free-breathing methodology independent of patient compliance is highly motivated. Studies on free-breathing bSSFP without contrast agent enhancement have shown high specificity, but lower sensitivity than what could be expected of CTA or Gd-MRA.^{4,5} Nyrén et al⁶ proposed a nonenhanced free-breathing methodology using repeated bSSFP acquisitions, and were able to show both high sensitivity and high specificity. However, reducing slice thickness for improved spatial resolution is hindered by flow artifacts. Spins flowing through the slice will accumulate a phase shift during the slice-selection gradient, which will result in erroneous spatial encoding, whereas spins entering the slice will experience a reduced number of RF pulses and will introduce steady-state signal perturbation.^{7,8} Disruption of the steady state and phase modulation will result in artifacts along the phase-encoding direction, potentially obscuring anatomy. Breathing motion will also aggregate erroneous spatial encoding, corrupting the image in areas that may be unaffected by flow artifacts. However, by using thicker slices and making repeated acquisitions to capture different phases of the cardiac and respiratory cycles, Nyrén et al showed that it is possible to largely circumvent these problems at the expense of a 5-fold prolonging of the imaging time.⁶ In this work, we propose that a 2D radial k-space trajectory could be used to simultaneously reduce both the flow and motion artifacts, as this kind of trajectory is known to be robust to motion⁹ and is intrinsically flow compensated for in-plane flow between TRs.¹⁰

The purpose of this work is to evaluate the feasibility of improving the nongated free-breathing non-contrast-enhanced

bSSFP methodology for imaging the pulmonary vasculature using a radial acquisition scheme with golden-angle radial ordering.

2 | METHODS

Healthy volunteers with no reported history of pulmonary disease ($n = 10$, age 46 ± 11 years, 50% female) were recruited to undergo MRI. In addition, patients with acute pulmonary embolism confirmed with CTA and D-dimer ($n = 2$, age 27 and 84, both female). The time between MRI and CTA was approximately 3 hours. The study was performed in agreement with the Helsinki Declaration and approved by the regional ethics board. Written, informed consent was obtained from both volunteers and patients.

2.1 | Pulse sequence

The pulse sequence used in this work was based on a standard 2D bSSFP pulse sequence for cardiovascular use. It was modified to allow for continuous acquisition with a golden-angle radial trajectory,¹¹ where the azimuthal angle of each readout is given by

$$\phi_{n+1} = \text{mod} \left[\phi_n + \pi \frac{\sqrt{5}-1}{2}, 2\pi \right]. \quad (1)$$

By using constant angular increment derived from the golden ratio, a nearly uniform coverage of k-space is obtained for an arbitrary number of spokes. To avoid artifacts that arise from undersampling of a radial trajectory, the Nyquist limit must be fulfilled in all parts of k-space (i.e., the distance between spokes at the edge of k-space must match the sampling distance along the spokes such that

$$P = \frac{M\pi}{2}, \quad (2)$$

where P is the number of spokes, and M is the matrix size. This relation is approximately valid also for golden-angle radial, particularly when the number of spokes is a Fibonacci number.¹¹

2.2 | Numerical simulations

To isolate the trajectory dependent effects of flow sensitivity, a numerical, voxel-based phantom was constructed in MATLAB (MathWorks, Natick, MA). A simplified anatomy was constructed as a transversal slice depicting the thoracic cavity including the ascending aorta, descending aorta, and the right pulmonary artery. The simulation was performed with a time step representing 1 TR. Each TR, 2 circles representing the aorta, was given a normal distributed random phase with opposing signs to simulate through-slice flow. An intensity

modulation, proportional to the phase shift but with equal sign, was added to the magnitude of the image to simulate in-flow of unsaturated spins. Noise was added to the signal to simulate the noise in MR images, resulting in Rician distributed magnitude signal. Sampling masks corresponding to a Cartesian phase-encoding line and a golden-angle radial spoke was constructed per TR and was used to sample the numerical phantom in the frequency domain. A total of 288 readouts were acquired for both methods. Density compensation for the golden-angle radial acquisition was performed by division with the sum of all radial sampling masks.

2.3 | Image acquisition

In vivo images were acquired with a 1.5T MRI scanner (Aera, Siemens Healthineers, Erlangen, Germany) using 34 surface coil elements. The acquisition was designed to compare free-breathing bSSFP imaging using the proposed golden-angle radial trajectory to the methodology proposed by Nyrén et al using a Cartesian trajectory, but without multiple repetitions, and at 3-mm slice thickness. The images were acquired in 2 series: once with the Cartesian trajectory (TE/TR: 1.6/3.2 ms, GRAPPA reduction factor 2, 163 lines of which 38 were autocalibration lines, sequential-linear phase encoding) and once with the golden-angle radial trajectory (TE/TR: 1.8/3.6 ms, SPIRiT, 1345 radial spokes, retrospectively subsampled to 144 and 610 consecutive spokes). The retrospective subsampling to 144 spokes was chosen to match the acquisition time of the Cartesian protocol, whereas 610 spokes was chosen as the Fibonacci number closest to the Nyquist limit for radial acquisitions (see Equation 2). The acquisition time per slice was 522 ms for the Cartesian acquisition and 4842 ms for the radial acquisition, retrospectively undersampled to 2196 and 518 ms. The temporal windows correspond approximately to an entire respiratory cycle, half of a respiratory cycle, and half of a cardiac cycle. The resulting total imaging time was approximately 40 seconds for the Cartesian acquisition and approximately 340 seconds, 150 seconds, and 40 seconds for the radial acquisitions, respectively. All other scan parameters were the same for both acquisitions, with relevant parameters as follows: flip angle = 60°; bandwidth = 1008 Hz/px; FOV = 450 × 450 mm²; matrix size = 288 × 288; voxel size = 1.6 × 1.6 × 3 mm³; slice thickness = 3 mm; and 70 contiguous slices in the transversal plane.

In 1 of the volunteers, 20 additional slices covering the left and right pulmonary arteries were acquired with the same parameters under free breathing, with end-expiratory breath-holding, with electrocardiogram (ECG) triggering, and with both end-expiratory breath-holding and ECG triggering. The images were acquired using sequential-linear and centric-interleaved phase-encoding schemes. An extended

scan protocol consisting of 10 000 spokes, corresponding to 36 seconds per slice, was evaluated in 1 healthy volunteer.

2.4 | Image reconstruction

The Cartesian images were reconstructed online on the scanner using GRAPPA, with a reduction factor of 2. The GRAPPA calibration was performed from 38 integrated autocalibration lines. Image intensity normalization of the Cartesian images was performed by the vendor-provided image normalization algorithm as part of the online reconstruction. The reconstruction of the radial images was implemented in MATLAB. The acquired data were reconstructed using the SPIRiT parallel imaging algorithm,¹² which is a minimization problem on the form

$$\hat{\mathbf{x}} = \arg \min_{\mathbf{x}} \{ \| \mathbf{D}\mathbf{x} - \mathbf{y} \|_2 + \lambda \| \mathbf{G}\mathbf{x} - \mathbf{x} \|_2 \} \quad (3)$$

where $\hat{\mathbf{x}}$ is the reconstructed image, \mathbf{D} is the sampling operator that maps the image onto the radial k-space, \mathbf{y} is the sampled data, and \mathbf{G} is the SPIRiT kernel. The calibration was made from the 30 centermost pixels of the radial k-space from which a 9 × 9 SPIRiT kernel was estimated. Image intensity normalization of the radial images was achieved using adaptive coil combination.^{13,14}

2.5 | Quantitative analysis of the images

To assess the ability to identify blood clots in patients, 2 patients with acute pulmonary embolism were scanned with the same protocol as the healthy volunteers. Blood-to-blood clot contrast, or blood clot visibility, was determined as

$$C_{\text{blood,clot}} = \frac{S_{\text{blood}} - S_{\text{clot}}}{S_{\text{blood}} + S_{\text{clot}}} \quad (4)$$

where S is the mean signal intensity within a region of interest in the clot and the blood surrounding the clot, respectively. To evaluate the sharpness of the pulmonary vessels, the system point spread function during motion should be considered. In practice, the full width at half maximum of the point spread function is often used to classify an imaging system, but reliably measuring the point spread function in vivo is impractical. Instead, the Deriche algorithm¹⁵ has been suggested for measurement of vessel sharpness.¹⁶ The algorithm uses a recursive filter to find the first-order derivative, yielding an edge image in which the magnitude of the image corresponds to the local derivative. By measuring an intensity profile of the Deriche image perpendicular to a vessel, the relative sharpness of the vessel can be estimated. The vessel sharpness measurement was normalized to the theoretical maximum and is represented in arbitrary units. Vessel sharpness was measured in the left and right main pulmonary artery and in segmental and subsegmental arteries that could easily be identified in both Cartesian and radial images.

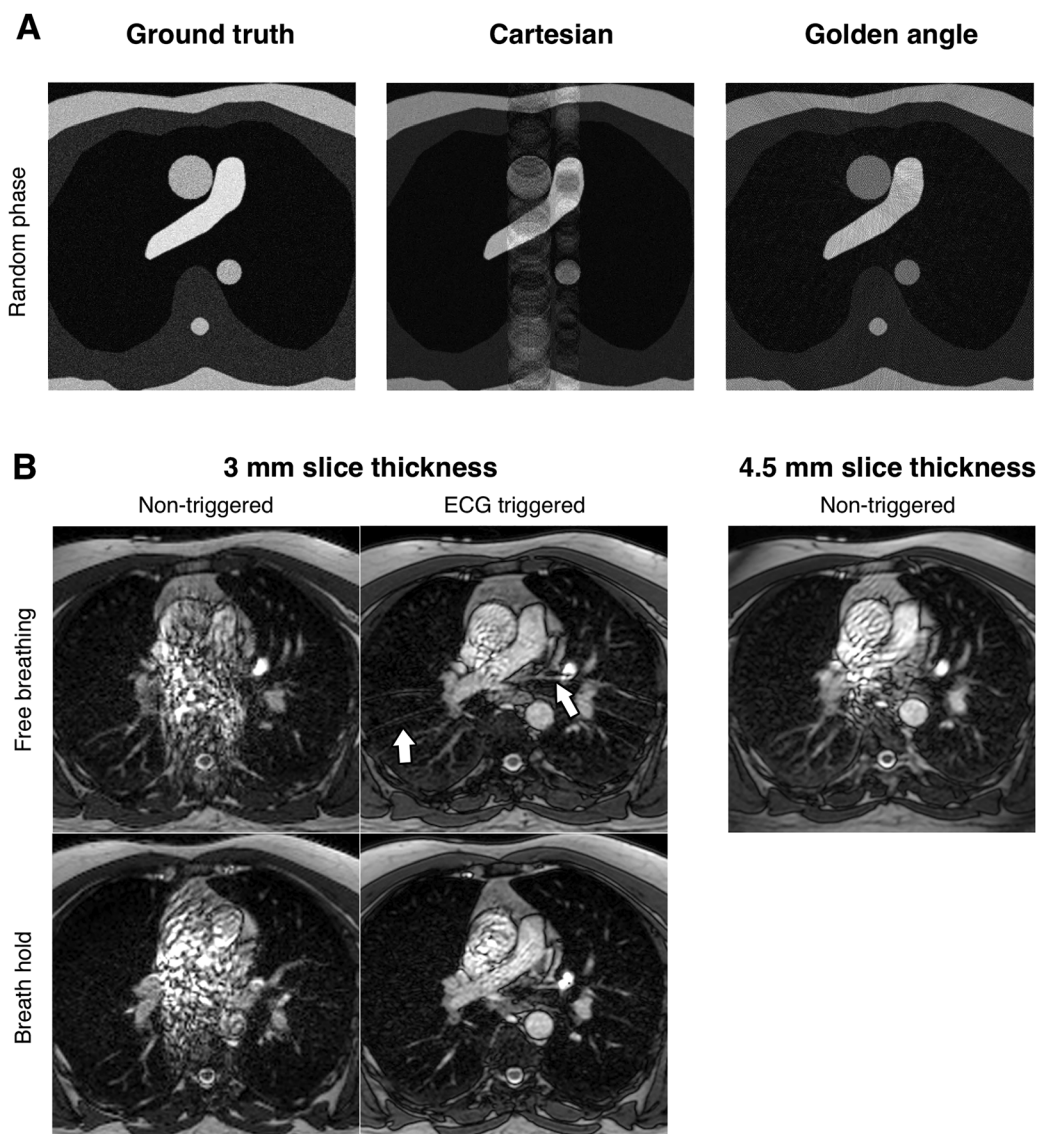


FIGURE 1 Limitations of Cartesian imaging of pulmonary vasculature. A, Simulations of trajectory response to random phase perturbation. The Cartesian trajectory (middle) exhibits artifacts along the phase-encoding direction of the image, whereas the golden-angle trajectory (right) exhibits an increased noise level compared with the ground truth (left) but does not show coherent artifacts obscuring the anatomy. B, In vivo measurements illustrating challenges with Cartesian acquisitions. Nontriggered acquisitions (left column) result in flow artifacts regardless of breath-holding. Electrocardiogram (ECG) triggered imaging during free breathing reduces the flow artifacts, but results in respiratory artifacts caused by discontinuities in k-space (top center). The flow artifacts are also reduced when acquiring thicker slices (top right), which indicate that most of the artifacts stem from the flow sensitivity of the slice-encoding gradient. Combining ECG triggering with breath-holding removes the artifacts, but is impractical as a result of the scan time limitations of multislice acquisitions

2.6 | Qualitative analysis of the images

The image series were anonymized and randomly mixed before being reviewed by 2 radiologists using the freely available ViewDEX software package.¹⁷ The observers were shown a stack of 70 slices imaged with 1 of the 2 methods. No identifying information was provided and there was no indication as to which method was the reference method and which was the tested method. The observers were asked to indicate their confidence that the images exhibited sufficient diagnostic quality and that the vessel sharpness and artifact

levels were acceptable for clinical use. As the scoring was done on healthy volunteers, diagnostic quality should be interpreted as the confidence with which the observers could declare the volunteers to be healthy. The score of 1 signified “not at all confident” and the score of 5 signified “completely confident.” Thus, the scores belonged to a scale that was ordinal, but not necessarily interval spaced. The observers were allowed to give different scores in the mediastinum, hilum, and lobar-level, segmental-level, and subsegmental levels of the pulmonary vasculature, but the scores were

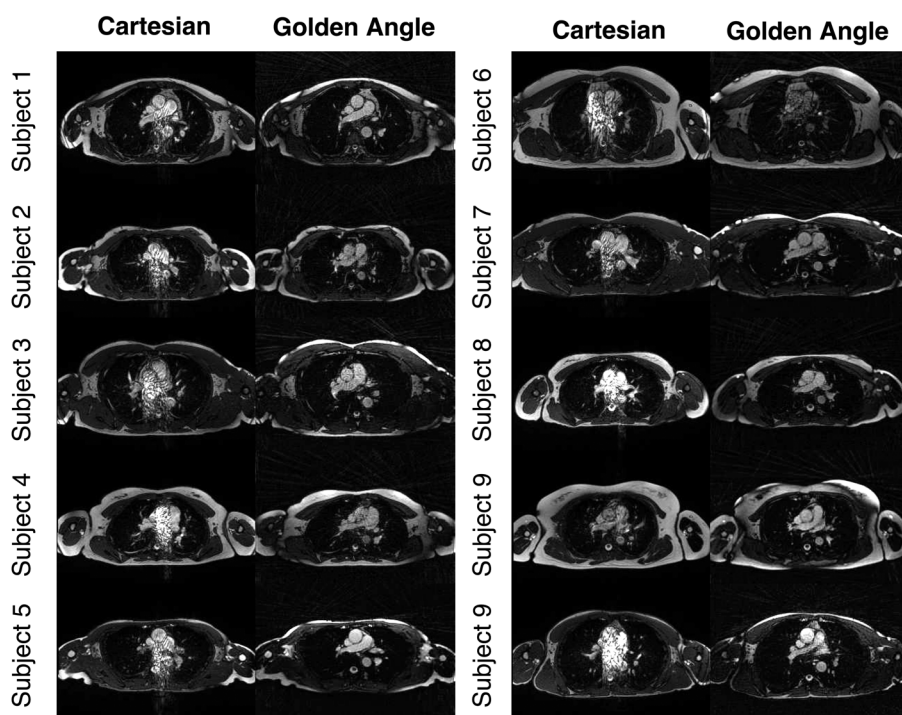


FIGURE 2 Representative slices from all subjects show that the left and right pulmonary arteries are obscured as a result of severe flow artifacts in all Cartesian acquisitions (images to the left), while little few artifacts are discernible in the golden-angle radial acquisitions (images to the right). However, the streaking artifacts that result from radial undersampling are discernible in the radial images

pooled prior to analysis. Image artifacts were classified as “flow- and breathing artifacts,” which originated from anatomy and physiology, or “undersampling artifacts,” which originated from the measurement methodology.

2.7 | Statistical analysis

Analysis of the observer’s scores was done using Visual Grading Characteristics (VGC)¹⁸ in the freely available VGC Analyzer software package.^{19,20} Visual Grading Characteristics is a nonparametric, rank, invariant method for statistical analysis of observer-reported image criteria scores (ICS). The ICS is a reflection of how well the image in question fulfills the image criterion, and the analysis assesses how the proportion of the test condition images that are scored higher than a certain threshold varies with the proportion of the reference condition, when the threshold is changed.¹⁸ A nonunitary ratio indicates a difference in confidence and an area under the cumulative distribution curve significantly greater than 0.5 indicates a significantly higher confidence in the test condition.²⁰ In each image criteria class, the Cartesian trajectory was considered the reference condition, and the radial trajectory the test condition. In addition to the VGC analysis, the Wilcoxon signed-rank sum test was chosen to compare the ICSs directly. Interobserver agreement was assessed using Spearman’s rank correlation coefficient (ρ). Continuous data are presented as mean \pm SD. A p value less than .05 was considered statistically significant.

3 | RESULTS

The image quality and diagnostic utility were hypothesized to be degraded by 2 separate processes, motion and flow, which both manifest as phase perturbations in the images. The numerical simulations show a considerably higher sensitivity to random phase perturbations in the Cartesian trajectory compared with the golden-angle radial trajectory (Figure 1A). In vivo acquisitions using a Cartesian trajectory under free breathing, with end-expiratory breath-holding, with ECG triggering, and with both end-expiratory breath-holding and ECG triggering, showed that most of the artifacts can be reduced by using ECG triggering (Figure 1B), suggesting that the largest contribution of phase perturbations originate from flow. Although nongated imaging will always be affected by some degree of movement, breath-holding had little effect on the image quality in the Cartesian images. However, ECG triggering increased respiratory-motion artifacts in Cartesian images unless used in combination with breath-holding.

Of the slices containing right and left main pulmonary arteries, 99 of 103 (96%) Cartesian images exhibited flow and breathing artifacts, compared with 7 of 103 (7%) for golden-angle radial (Figure 2). One case (Figure 2, subject 6) had artifacts that were perceived to be detrimental to the diagnostic utility in both the radial and Cartesian acquisitions. All of the radial images exhibited some degree of undersampling artifacts, whereas none of the Cartesian

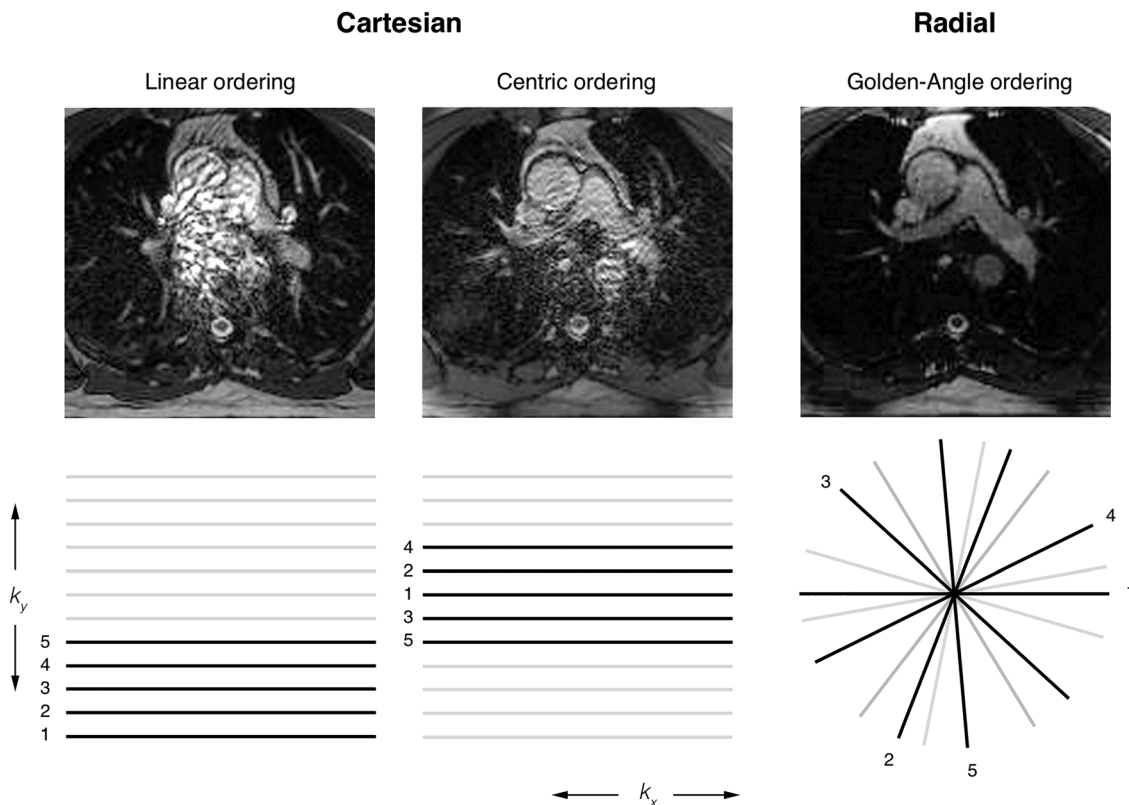


FIGURE 3 Effects of k -space trajectory ordering on flow artifacts. The artifacts take on a different appearance depending on the phase-encoding ordering used. Using a conventional sequential-linear Cartesian ordering, in which the phase-encoding lines are continuously ordered in the k_y direction (left), the flow artifacts are very prominent. By using a quasi-random centric-interleaved phase-encoding ordering along the k_y direction (center), the effect of the phase errors can be averaged and becomes less disruptive, albeit still severe. By using a quasi-random golden-angle ordering along both k_x and k_y (right), the artifacts are effectively suppressed

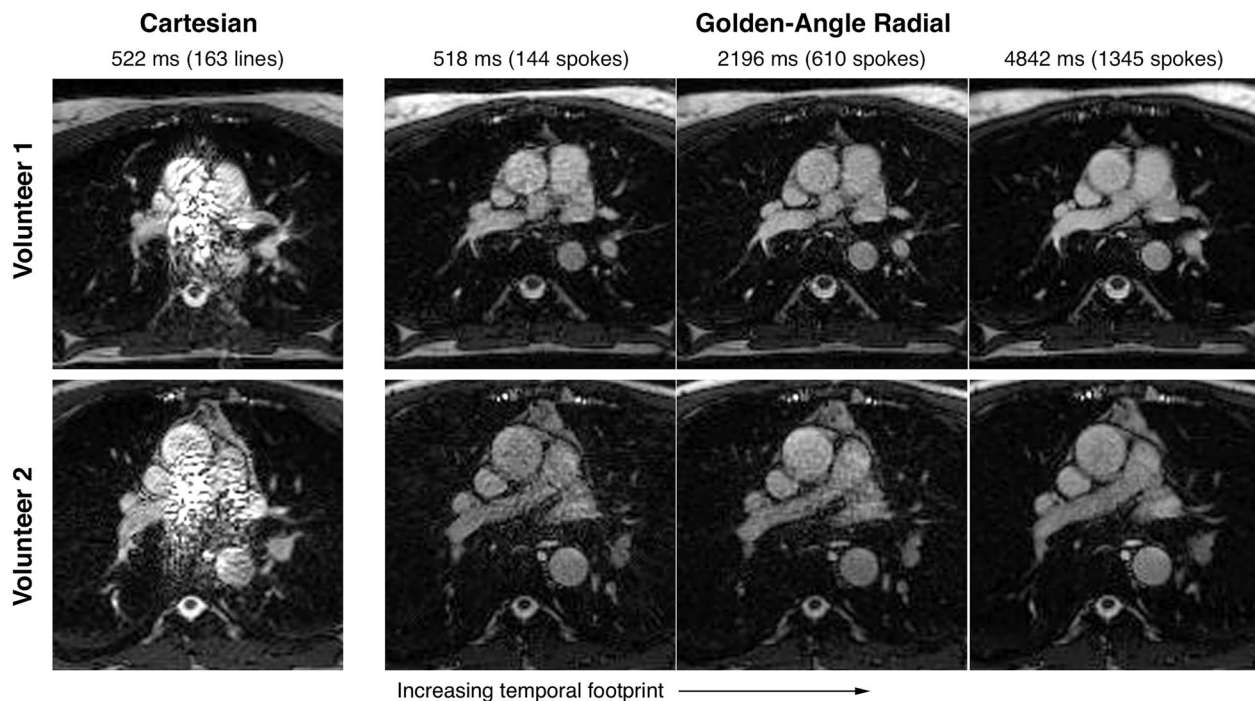


FIGURE 4 Images from 2 volunteers. Using a golden-angle radial acquisition permits reconstruction with multiple and flexible temporal footprints from the same acquisition. A small temporal footprint permits freezing motion at the expense of reduced SNR. Using different temporal footprints does not affect the robustness to flow. The effect of using larger temporal footprints is shown in Supporting Information Figure S1 and Video S2

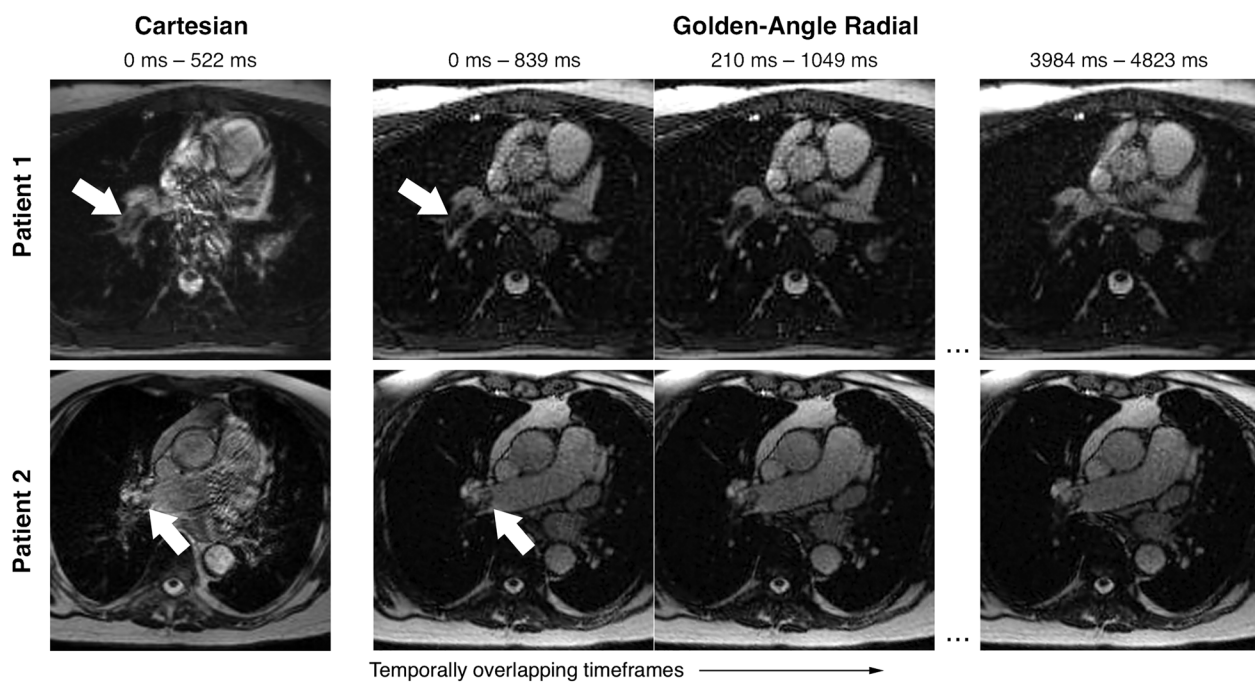


FIGURE 5 Sliding window reconstructions from golden-angle radial acquisitions in 2 patients. The flexibility of choosing data from the golden-angle acquisitions permits dynamic reconstructions. Here, a temporal footprint of 839 ms was arbitrarily chosen, corresponding to 233 radial spokes. A dynamic sliding window reconstruction was then performed with 75% (175 spokes) overlap between consecutive frames, achieving 19 frames from a 5-second acquisition. Arrows indicate the location of identified emboli. Videos from both patients are shown in Supporting Information Videos S3 and S4

images exhibited that kind of artifacts. The effect of the phase-encoding ordering is illustrated in Figure 3, where the centric-interleaved phase encoding exhibits different, albeit severe artifacts, whereas the radial trajectory is almost completely free of visible flow artifacts, mirroring the findings from Figure 1.

The utility of performing flexible temporal resolution sliding window reconstructions is illustrated in Figure 4, where the noise was reduced in the larger temporal footprint, but motion blurring or artifacts were not readily apparent. Expanding the temporal window further shows diminishing returns with respect to acquisition time (Supporting Information Figure S1 and Video S2). The flexibility of the golden-

angle trajectory is further illustrated in Figure 5 and Supporting Information Videos S3 and S4, where moving images show the location and movement of the emboli over the respiratory cycle. The quantitative analysis showed a higher vessel sharpness in the golden-angle radial images ($n = 76$, 0.79 ± 0.11 versus 0.71 ± 0.16 , $p < .05$). One subject was excluded from the central vessel measurement as a result of prohibitively poor image quality in the Cartesian images. The reduced blurring with radial imaging in the segmental and subsegmental branches of the pulmonary arteries is illustrated in Figure 6. Quantitative analysis of the contrast between blood and blood clot showed higher contrast for golden-angle radial in both patients (0.42 versus 0.20 and

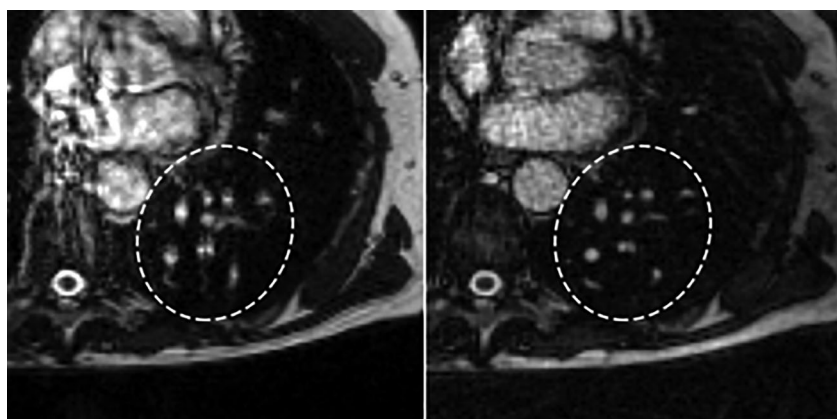


FIGURE 6 A close-up of segmental pulmonary vessels (dashed circle) indicates a clear difference in vessel sharpness between Cartesian (left) and golden-angle radial (right) in the same subject

Magnetic Resonance in Medicine

TABLE 1 Scores for all image series, pooled for image criteria

	Cartesian	Golden angle 144 spokes	610 spokes	1345 spokes
Diagnostic quality	2.2 ± 0.6	2.3 ± 0.7	2.8 ± 0.8	3.5 ± 0.9
Vessel sharpness	2.1 ± 0.5	2.2 ± 0.8	2.6 ± 0.9	3.4 ± 0.9
Artifacts	3.0 ± 1.0	3.0 ± 0.9	3.4 ± 0.8	3.9 ± 0.7

Note: Higher scores signify better images.

0.54 versus 0.30, difference 23% in both cases). The VGC analysis indicated higher confidence ($p < .05$) in golden-angle radial in the “diagnostic quality” and “vessel sharpness” classes, whereas “artifact level” did not differ ($p = .20$) for comparable temporal resolution. The corresponding ICS were higher in golden-angle radial in the “diagnostic quality” (2.3 ± 0.7 versus 2.2 ± 0.6, $p < .05$) and “vessel sharpness” (2.2 ± 0.8 versus 2.1 ± 0.5, $p < .05$) categories, whereas “artifact level” did not differ (3.0 ± 0.9 versus 3.0 ± 1.0, $p = .80$). The ICSs for all temporal footprints are presented in Table 1. Interobserver agreement for all ($n = 4960$) scores was calculated by Spearman’s sign-rank correlation and was found to be $\rho = 0.5$.

4 | DISCUSSION

The main finding of this study was that the image quality was increased by using a golden-angle radial sampling trajectory for imaging of pulmonary embolism when assessed by 2 radiologists.

In this study, we investigated the hypothesis that the images were degraded by motion and flow artifacts, which primarily prohibit diagnosis at small slice thicknesses. It was found that the artifacts could be reduced using ECG triggering at the expense of prolonging the scanning time. However, it was found that ECG triggering itself introduced more respiratory motion artifacts. Although motion robustness could be improved by using breath-holding, it would increase the scan time at least 2-fold, and would be dependent on patient compliance, which may not be feasible in the targeted patient population. Thus, the motion robustness alone may be able to offset the decrease in effectiveness associated with using a radial trajectory. By minimizing the need for patient preparation, the time from admission to diagnosis could potentially be shortened. Furthermore, the golden-angle radial methodology could be used to salvage MRA exams with poor bolus timing, as pulmonary emboli are not expected to exhibit enhancement after injection of Gadolinium-based contrast agents.

The methodology proposed in this study uses a 2D acquisition. All images shown in this study are acquired in the transversal plane. However, for diagnostic purposes,

perpendicular slices would be needed to improve confidence in identifying potential pathology, meaning that the acquisition would have to be repeated in the sagittal plane, the coronal plane, or both. This raises the question why multiple 2D acquisitions should be used instead of a single 3D acquisition. A 2D acquisition technique was chosen to be able to suppress motion, but also for the increased bright-blood contrast that can be attributed to inflow (i.e., lack of saturation). As supported by our findings, acute pulmonary emboli present as hypo-intense on bSSFP images; thus, the nonselective or slab-selective RF pulse used in 3D imaging would decrease the blood-to-blood clot contrast. Furthermore, slice misregistration is always a risk in 2D free-breathing acquisitions; therefore, a breath-held or respiratory/navigator triggered method may be preferable for maximum intensity projection reconstructions, regardless of the trajectory. However, in this manuscript, we suggest using the flexibility of the golden-angle radial trajectory to perform a sliding window reconstruction that mitigates the problem of slice misregistration altogether, as each slice is viewed independently, and through-plane motion is captured over the course of the respiratory cycle.

This preliminary, technical investigation is limited by the small sample size and the fact that the population consisted primarily of healthy volunteers and should merely be considered a proof of concept. To assess the diagnostic performance of golden-angle radial imaging for detection and diagnosis of pulmonary emboli, a larger clinical population of patients with suspected pulmonary emboli needs to be imaged and read by blinded observers with relevant subspecialization, including a comparison with an established gold standard.

The observer scoring showed no difference in artifact levels between the 2 methods, even though visual inspection showed a tangible difference (Figures 2–6). Because of the imperfect definition of an artifact, both obtrusive flow artifacts and benign streaking artifacts were likely taken into consideration by the observers, which could explain the observed discrepancy. However, the severity of the flow and streaking artifacts were likely reflected in the perceived diagnostic quality score, which was higher for the radial images. The qualitative analysis showed that nearly all of the

Cartesian images exhibited some degree of artifacts obscuring anatomy of particular clinical interest (i.e., the left and right main pulmonary arteries). However, even though the sample size was small, differences could be observed with statistical significance. As a result of technical limitations in the pulse sequence, the radial acquisition used a slightly longer TE and TR (difference of 0.4 ms), resulting in a slightly different location of the banding artifacts that are characteristic of bSSFP pulse sequences. This difference was most notable in Figure 1, subject 9. It is also possible that some image inhomogeneity may be attributed to eddy current effects, which may become an issue when using a golden-angle radial trajectory; however, initial experiments with double averaging,²¹ pairing,²² and smaller angular increments²³ showed no tangible difference in image quality *in vivo* (data not shown).

5 | CONCLUSIONS

In conclusion, the motion and flow robustness of a radial trajectory improves perceived diagnostic quality and vessel sharpness when imaging the pulmonary vasculature in healthy volunteers. The radial methodology allows for imaging with thinner slices compared with the Cartesian methodology without flow artifacts, meaning that steps are taken toward a safer way to diagnose suspected phase encodings, without compromising on the diagnostic utility.

ACKNOWLEDGMENT

This research was funded in part by the Swedish Foundation for Strategic Research (SSF ICA-120063) and the Stockholm County Council (ALF LS 1411-1372).

ORCID

Alexander Fyrdahl  <http://orcid.org/0000-0003-0237-7699>

REFERENCES

- [1] Goldhaber SZ, Bounameaux H. Pulmonary embolism and deep vein thrombosis. *Lancet*. 2012;379:1835-1846.
- [2] Stein PD, Fowler SE, Goodman LR, Gottschalk A, Hales CA, Hull RD, Leeper KVJ. Multidetector computed tomography for acute pulmonary embolism. *N Engl J Med*. 2006;354:2317-2327.
- [3] Stein PD, Chenevert TL, Fowler SE, et al. Gadolinium-enhanced magnetic resonance angiography for pulmonary embolism. *Ann Intern Med*. 2010;152:434-443.
- [4] Kalb B, Sharma P, Tigges S, et al. MR imaging of pulmonary embolism: diagnostic accuracy of contrast-enhanced 3D MR pulmonary angiography, contrast-enhanced low-flip angle 3D GRE, and nonenhanced free-induction FISP sequences. *Radiology*. 2012;263:271-278.
- [5] Revel MP, Sanchez O, Lefort C, et al. Diagnostic accuracy of unenhanced, contrast-enhanced perfusion and angiographic MRI sequences for pulmonary embolism diagnosis: results of independent sequence readings. *Eur Radiol*. 2013;23:2374-2382.
- [6] Nyrén S, Nordgren-Rogberg A, Vargas-Paris R, Bengtsson B, Westerlund E, Lindholm P. Detection of pulmonary embolism using repeated MRI acquisitions without respiratory gating: a preliminary study. *Acta Radiol*. 2017;58:272-278.
- [7] Markl M, Alley MT, Elkins CJ, Pelc NJ. Flow effects in balanced steady state free precession imaging. *Magn Reson Med*. 2003;903:892-903.
- [8] Bieri O, Scheffler K. Flow compensation in balanced SSFP sequences. *Magn Reson Med*. 2005;54:901-907.
- [9] Nishimura DG, Jackson J, Pauly JM. On the nature and reduction of the displacement artifact in flow images. *Magn Reson Med*. 1991;492:481-492.
- [10] Bieri O, Scheffler K. Fundamentals of balanced steady state free precession MRI. *J Magn Reson Imaging*. 2013;38:2-11.
- [11] Winkelmann S, Schaeffter T, Koehler T, Eggers H, Doessel O. An optimal radial profile order based on the golden ratio for time-resolved MRI. *IEEE Trans Med Imaging*. 2007;26:68-76.
- [12] Lustig M, Pauly JM. SPIRiT: iterative self-consistent parallel imaging reconstruction from arbitrary k-space. *Magn Reson Med*. 2010;64:457-471.
- [13] Walsh DO, Gmitro AF, Marcellin MW. Adaptive reconstruction of phased array MR imagery. *Magn Reson Med*. 2000;43:682-690.
- [14] Griswold M, Walsh D, Heidemann RM, Haase A, Jakob P. The use of an adaptive reconstruction for array coil sensitivity mapping and intensity normalization. In Proceedings of the 10th Annual Meeting of ISMRM, Honolulu, HI, 2002. p 2410.
- [15] Deriche R. Fast algorithms for low-level vision. *IEEE Trans Pattern Anal Mach Intell*. 1990;12:78-87.
- [16] Maintz D, Aepfelbacher FC, Kissinger KV, et al. Coronary MR angiography: comparison of quantitative and qualitative data from four techniques. *Am J Roentgenol*. 2004;182:515-521.
- [17] Håkansson M, Svensson S, Zachrisson S, Svalkvist A, Båth M, Månssohn LG. ViewDEX: an efficient and easy-to-use software for observer performance studies. *Radiat Prot Dosimetry*. 2010; 139:42-51.
- [18] Båth M, Månssohn LG. Visual grading characteristics (VGC) analysis: a non-parametric rank-invariant statistical method for image quality evaluation. *Br J Radiol*. 2007;80:169-176.
- [19] Båth M, Hansson J. VGC Analyzer: a software for statistical analysis of fully crossed multiple-reader multiple-case Visual Grading Characteristics studies. *Radiat Prot Dosimetry*. 2016; 169:46-53.
- [20] Hansson J, Månssohn LG, Båth M. The validity of using ROC software for analyzing Visual Grading Characteristics data: an investigation based on the novel software VGC Analyzer. *Radiat Prot Dosimetry*. 2016;169:54-59.
- [21] Markl M, Leupold J, Bieri O, Scheffler K, Hennig J. Double average parallel steady-state free precession imaging: optimized eddy current and transient oscillation compensation. *Magn Reson Med*. 2005;974:965-974.
- [22] Bieri O, Markl M, Scheffler K. Analysis and compensation of eddy currents in balanced SSFP. *Magn Reson Med*. 2005;54: 129-137.

- [23] Wundrak S, Paul J, Ulrici J, Hell E, Rasche V. A small surrogate for the golden angle in time-resolved radial MRI based on generalized fibonacci sequences. *IEEE Trans Med Imaging*. 2015;34:1262-1269.

SUPPORTING INFORMATION

Additional Supporting Information may be found in the supporting information tab for this article.

FIGURE S1 Supporting figure to Figure 4. Increasing temporal footprints show diminishing returns with respect to time.

VIDEO S2 Supporting video to Figure 4. Increasing temporal footprints show diminishing returns with respect to time.

VIDEO S3 Supporting video to Figure 5. Sliding window image showing an embolus in the right pulmonary artery of a 27-year-old female.

VIDEO S4 Supporting video to Figure 5. Sliding window image showing an embolus in the right pulmonary artery of an 84-year-old female.

How to cite this article: Fyrdahl A, Vargas Paris R, Nyrén S, et al. Pulmonary artery imaging under free-breathing using golden-angle radial bSSFP MRI: a proof of concept. *Magn Reson Med*. 2018;80:1847–1856. <https://doi.org/10.1002/mrm.27177>